Influence of steel grain size on residual stress in grinding processing

doi: 10.4028/www.scientific.net/MSF.638-642.2389

Influence of Steel Grain Size on Residual Stress in Grinding Processing

M. Gotoh[1,a], K. Seki[1,b], M. Shozu[2,c], H. Hirose[3,d] and T. Sasaki[1,e]

[1]Graduate school of Natural Science and Technology, Kanazawa University,
Kakuma, Kanazawa, Ishikawa, 9201192, Japan

[2]Department of Mechanical Engineering, Maizuru National College of Technology,
234, Azasiroya, Maizuru, Kyoto, 6258511, Japan

[3]Kinjo University,
Kasama, Hakusan, Ishikawa, 9248511, Japan

[a]masahide@cs.s.kanazawa-u.ac.jp, [b]katuhiro@kenroku.kanazawa-u.ac.jp,
[c]shozu@maizuru-ct.ac.jp, [d]hirose@kinjo.ac.jp, [e]sasakit@kenroku.kanazawa-u.ac.jp

Keywords: Residual stress, X-ray stress measurement, Fine-grained steel, Grind, Polish.

Abstract. The fine-grained rolling steels NFG600 and the conventional usual rolling steels SM490 were processed by sand paper polishing and mechanical grinding to compare the residual stress generated after processing. The average grain size of NFG600 and SM490 is 3 μm and 15μm respectively. Therefore improvement of mechanical properties for such fine-grained steels is expected, it is important to understand the residual stress state of new fine-grained materials with processing. In this study, multi axial stresses of two kinds of specimens after polishing and grinding were measured by three kinds of analysis methods including cos-ψ method. As a result, as for σ_{33}, the stress of NFG was compression, though that of SM490 was tension.

Introduction

In general, fine-grained steels are expected to have higher mechanical properties than conventional steels according to Hall-Petch relation. Nakayama steel works, Ltd. in Japan developed the fine-grained rolling steels named 'Nakayama Fine Grain (NFG)' as commercial materials [1]. Specific property of this steel is that the grain size is about 3 μm, which is one-third smaller than conventional steels. Therefore, the tensile strength becomes 1.5 times stronger. Naturally, the hardness becomes high, and the wear resistance and fatigue life are also improved. In addition, ductile-to-brittle transition temperature (DBTT) is lower than that of conventional one.

In the practical use of steel, processing like machining or grinding affects on the surface layer of steel. Therefore it is important to understand the residual stress state of new fine-grained materials. Some researcher investigated the surface residual stress state of grinded steels using X-ray stress measurement in past. Hanabusa et al. described that the ratio of the X-ray penetration depth to the distance between second particles or cell walls is important to decide tri-axial components [2]. Thus, the semblance tri-axial residual stress generated in fine-grained steel would be different from that in conventional steel, because the ratio of the X-ray penetration depth to the distance between grain walls in fine-grained steel is high compared with conventional steel.

In present study, specimens of NFG steel and conventional JIS-SM490 steel were prepared. The chemical composition of two materials is the same. Then, two kinds of similar mechanical processing were given to both specimens. The residual stresses of specimens ground and polished were obtained by X-ray stress measurement through three kinds of analysis methods.

Experimental

Materials. Fine-grained rolling steels that are named NFG600 by Nakayama Steel Works, Ltd. and conventional Mn rich steels that are named SM490 in Japanese Industrial Standard were used in present study. SM490 is an initial material of NFG600 that is refined by severe plastic deformation and quick quenching [1]. The chemical composition of two materials is the same, as shown in table 1. Figure 1 shows microstructures of materials. The structure of both materials was dual phase structure consisted of ferrite and pearlite, however, each average grain size was different. The average grain size of NFG600 and SM490 were 3 μm and 15 μm respectively. Accordingly, mechanical properties of NFG600 were different from SM490 as expected by Hall-Petch relation. Mechanical properties obtained by tensile test and micro Vickers hardness test are summarized in table 2.

Table 1. Chemical composition of present material [weight %].

C	Si	Mn	P	S
0.17	0.36	1.30	0.011	0.007

Table 2. Mechanical properties by tensile and hardness test.

	Yield stress, [MPa]	Ultra tensile strength, [MPa]	Total elongation, [%]	Vickers hardness, [GPa]
NFG600	428	560	26	2.0
SM490	336	500	29	1.4

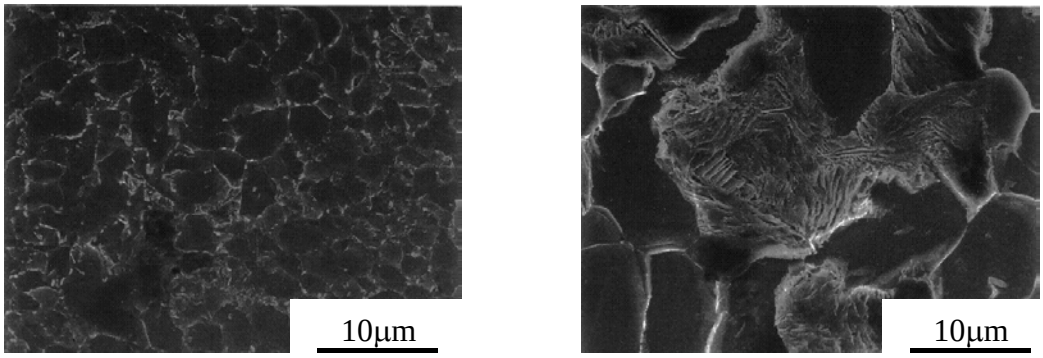

(a) NFG600 (d_{avr}=3μm) (b) SM490 (d_{avr}=15μm)

Figure 1. Microstructures of materials.

Directional Processing by Grinding and Polishing. Both NFG600 and SM490 were processed with grinding machine and sanding in order to give the residual stress in the materials. The specimens were cut out to the dimension of 60 mm in length, 10 mm in width and 5 mm in thickness before processing, and influenced layer under 0.2 mm from surface by machining was removed by electrochemical polishing. As for the condition of grinding, specification of grinding wheel is 180x13UW60KV58, width of grinding wheel was 13 mm, spindle speed is 3460 rpm, table feed speed is 170 mm/sec and cutting depth is 5 μm/pass. After a grinding wheel ground the specimen in depth of 5 μm all at once, it got there and backed twice while holding depth of cut. An emulsion for cooling was not used in grinding processing. As for polishing processing, the specimen was polished by SiC #1200 sand paper to one direction 1000 times.

X-ray Stress Measurements. Stress measurements on the specimens were carried out by X-ray diffraction to know influence on the residual stress of grain sizes. Major conditions of X-ray diffraction on the stress measurement are shown in table 3. Figure 2 shows the coordinate system of X-ray stress measurement. Although conventional X-ray plane stress analysis [3] was applied by $\sin^2\psi$ method, tri-axial stress analysis was also carried out by Dölle-Hauk method and cos-ψ method [4]. Lattice strain $\varepsilon_{\phi\psi}$ by means of X-ray on the coordinate system in fig.2 is

Table 3. Conditions of X-ray diffraction experiments.

Radiation	Cr-Kα
Diffraction line	Fe211
Diffraction angle $2\theta_0$, [deg]	156.45
Tube voltage, [kV]	200
Tube current, [mA]	10
Irradiate area, [mm^2]	4x6
Number of angle ψ	7
Elastic constant E, [GPa]	221.5
Poison ratio	0.27
Linear absorption coef., [μm^{-1}]	8.3x10^{-2}

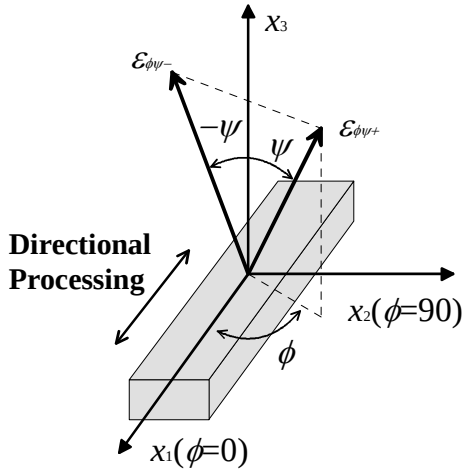

Figure 2. Coordinate system of experiments.

$$\varepsilon_{\phi\psi}=\frac{1+\nu}{E}[(\sigma_{11}\cos^2\phi+\sigma_{12}\sin 2\phi+\sigma_{22}\sin^2\phi)\sin^2\psi$$
$$+\sigma_{33}\cos^2\psi+(\sigma_{13}\cos\phi+\sigma_{23}\sin\phi)\sin 2\psi]-\frac{\nu}{E}(\sigma_{11}+\sigma_{22}+\sigma_{33}). \quad (1)$$

In conventional $\sin^2\psi$ method, ϕ=0, $\sigma_{13}/\sigma_{23}/\sigma_{33}$=0 are adopted because of assumption of plane stress state. In tri-axial stress analysis by Dölle-Hauk method, the average strain a_1 and the deviation a_2 are defined by using Eq.1 as

$$a_1=\frac{\varepsilon_{\phi\psi+}+\varepsilon_{\phi\psi-}}{2}=\frac{1+\nu}{E}[(\sigma_{11}\cos^2\phi+\sigma_{12}\sin 2\phi+\sigma_{22}\sin^2\phi)\sin^2\psi$$
$$+\sigma_{33}\cos^2\psi]-\frac{\nu}{E}(\sigma_{11}+\sigma_{22}+\sigma_{33}), \quad (2)$$
$$a_2=\frac{\varepsilon_{\phi\psi+}-\varepsilon_{\phi\psi-}}{2}=\frac{1+\nu}{E}(\sigma_{13}\cos\phi+\sigma_{23}\sin\phi)\sin 2\psi. \quad (3)$$

According to Eq.2 and 3, a_1 and a_2 should have the linear relation with $\sin^2\psi$ and $\sin 2\psi$ respectively. Hence, tri-axial stress components σ_{13}, σ_{23} are obtained by the slope of a_2 vs. $\sin 2\psi$ directly when ϕ=0^o and 90^o are assigned to Eq.3. Additionally, ε_{33} can be calculated by the diffraction angle at ψ=0^o, therefore, components σ_{11}, σ_{22}, σ_{33} and σ_{13} are obtained by the slope of a_1 vs. $\sin^2\psi$ when ε_{33}, ϕ=0^o and 90^o are assigned to Eq.2. In cos-ψ method, it is assumed that each stress component has a liner stress gradient along depth z. The stress at z under a multiaxial stress state σ_{ij} is

$$\sigma_{ij}(z)=\sigma_{ij0}+A_{ij}=\begin{bmatrix}\sigma_{110} & \sigma_{120} & 0\\ & \sigma_{220} & 0\\ & & 0\end{bmatrix}+\begin{bmatrix}A_{11} & A_{12} & A_{13}\\ & A_{22} & A_{23}\\ & & A_{33}\end{bmatrix}z, \quad (4)$$

where σ_{ij0} is a stress on the surface (z=0) and A_{ij} is stress gradient. In X-ray stress measurement, the weighted average stress $<\sigma_{ij}>$ is measured in practice.

$$<\sigma_{ij}>=\int_0^{z_1}\sigma_{ij}(z)I(z)dz\,/\int_0^{z_1}I(z)dz=\int_0^{z_1}\sigma_{ij}(z)\exp(-z_1/T)dz/\int_0^{z_1}\exp(-z_1/T)dz$$
$$=\sigma_{ij0}+A_{ij}T\frac{\exp[-z_1/T](1+z_1/T)-1}{\exp[-z_1/T]-1}$$

$$= \sigma_{ij0} + A_{ij} TW, \tag{5}$$

where W is the weighted factor, which is 0.42 in the case of $z_1=T$. T is the penetration depth of X-ray defined by

$$T=\frac{\sin^2\theta-\sin^2\psi}{2\mu\sin\theta\cos\psi}=T_1\frac{1}{\cos\psi}+T_2\cos\psi. \tag{6}$$

In Eq.2 and 3, a_i and σ_{ij} can be changed to $<a_i>$ and $<\sigma_{ij}>$. By Eq.5 and 6 and this new equation using Eq.2 and 3, $<a_1>$ and $<a_2>$ are expressed as new function including $\cos\psi$. Since this new equation can treat with strain $\varepsilon_{\phi\psi}$ only, it can be changed to new expression with diffraction angle 2θ by the equations as follows:

$$<a_1>'=\frac{1}{2}[<2\theta_{\psi+}>+<2\theta_{\psi-}>]=-2\tan\theta_0<a_1>+2\theta_0, \tag{7}$$

$$<a_2>'=\frac{1}{2}[<2\theta_{\psi+}>-<2\theta_{\psi-}>]=-2\tan\theta_0<a_2>, \tag{8}$$

$$<\varepsilon_{\phi\psi}>'=<2\theta_{\phi\psi}>=-2\tan2\theta_0<\varepsilon_{\phi\psi}>+2\theta_0. \tag{9}$$

where θ_0 is the diffraction angle of stress free state. Then, $<a_1>'_{at\ \phi=0}+<a_1>'_{at\ \phi=90}$ and $<a_1>'_{at\ \phi=0}-<a_1>'_{at\ \phi=90}$ are obtained as

$$<a_1>'_{at\ \phi=0}+<a_1>'_{at\ \phi=90}=(\sigma_{110}+\sigma_{220})X_1+(A_{11}+A_{22})X_2+A_{33}X_3+2(2\theta_0), \tag{10}$$

$$<a_1>'_{at\ \phi=0}-<a_1>'_{at\ \phi=90}=(\sigma_{110}-\sigma_{220})X_4+(A_{11}-A_{22})X_5, \tag{11}$$

$$X_1=-2\tan\theta_0[-(1+\nu)\cos^2\psi+(1-\nu)]/E, \tag{12}$$

$$X_2=X_1(T_2\cos\psi+T_1/\cos\psi)W, \tag{13}$$

$$X_3=-4\tan\theta_0[(1-2\nu)(T_2\cos\psi+T_1/\cos\psi)W]/E-2X_2, \tag{14}$$

$$X_4=-2\tan\theta_0[(1+\nu)\sin^2\psi]/E, \tag{15}$$

$$X_5=X_4(T_2\cos\psi+T_1/\cos\psi)W. \tag{16}$$

Because X_i is a constant, several expressions corresponding to the number of angles ψ can be obtained. This problem can be solved by multiple regression analysis, σ_{110}, σ_{220}, A_{11}, A_{22} and A_{33} can be calculated by Eq.10 and 11 finally. Similarly, σ_{120}, A_{12}, A_{13} and A_{23} can be calculated from $<a_1>'_{at\ \phi=0}-<a_1>'_{at\ \phi=90}$, $<a_1>'_{at\ \phi=45}+<a_1>'_{at\ \phi=-45}$ and $<a_1>'_{at\ \phi=45}-<a_1>'_{at\ \phi=-45}$. Residual stresses of freshly-created surface were measured after removing old surface every 10 μm in depth by electro-chemical polishing.

Results and Discussion

Figure 3 shows 2θ-$\sin^2\psi$ diagrams obtained by the stress measurement. It's common knowledge generally that compressive residual stresses appear by polishing and tensile residual stresses generate by mechanical grinding, and results obtained from the diagrams using conventional $\sin^2\psi$ method were agreed with this knowledge. The ψ-split phenomenon was clearly observed in grinding specimens. Since the ψ-split did not appear in the figure of $\phi=90^o$, it means $\sigma_{23}=0$ in Dölle method.

Stress values of processed surface obtained by $\sin^2\psi$ method and Dölle method are shown in table 4 and table 5 respectively. As a result of $\sin^2\psi$ method, σ_{11} (also σ_{22}) depended on the angle ϕ because the slope of $\sin^2\psi$ diagram was different by ψ-split. In addition, differences of stresses between materials were really small. However, as a result of Dölle method, σ_{11} and σ_{22} of polishing were different by each material because of influence of σ_{33} on σ_{11} and σ_{22}. Here, the X-ray

penetration depth z at ψ=0° is about 5.8 μm calculated by Eq.6. The ratio of the depth z to the distance l between grain walls ($d_{avr.}$=15 μm) in SM490 is around 2:5. For NFG600, they are in the ratio 3:1. Hanabusa et al. described in the reference [2] that the relaxation of stresses due to the surface effect is less than 10 % at z=0.5l and completely negligible below the depth of the order of the inter-particle spacing. In the case of SM490, the relaxation of stresses by the surface effect is less than 20%, moreover, there is a possibility that second particles are distributed in a grain. Therefore, it would be difficult to distinguish the effect of grain size from the effect of mechanical properties such as hardness for the fundamental of occurrence of σ_{33}. However, although the damage to specimen with grinding is pretty terrible, the relaxation of stresses mentioned above could appear because the difference of stress in polishing between two materials is larger than that in grinding. Table 6 shows stress components of processed surface obtained by cos-ψ method. It seems that the difference of stress value between σ_{110} and σ_{220} were larger than that obtained by other methods. Moreover, these values were larger compared with other methods because it take the effect due to stress gradient into account. Particularly, it is should be noted that the discrimination of A_{33} between NFG600 and SM490 became clearer. Furthermore, although σ_{33} of NFG600 were negative values in the case of Dölle method, the A_{33} by cos-ψ method were positive values. It would mean that alternation of the sign exists from 0 μm to 10 μm in depth. Actually, in grinding, A_{33} of NFG600 at 10 μm under was -8.5 MPa/μm, that of SM490 was also 15.2 MPa/μm. Figure 4 shows distributions to depth of the normal residual stress σ_{33} by calculation from A_{ij} MPa/μm and by Dölle method. The stresses by Dölle method was estimated small compared with actual stresses, because the effect of free surface was not considered. However, it is interesting that the sign of stress values was different from each other. As seen above, the multi axial stress analysis involved gradient components is very useful to know the stress status generated by mechanical processing.

Table 4. Results by $\sin^2\psi$ method of processed surface [MPa].

		$\sigma_{11}(\phi=0^o)$	$\sigma_{22}(\phi=90^o)$	$\sigma_{11}(\phi=180^o)$	$\sigma_{22}(\phi=-90^o)$
NFG600	Polishing	-221.6	-207.2	-196.3	-198.0
	Grinding	333.1	173.3	375.8	165.9
SM490	Polishing	-226.5	-201.4	-211.4	-200.2
	Grinding	325.0	154.9	389.2	153.8

Table 5. Results by Dölle method of processed surface [MPa].

		σ_{11}	σ_{22}	σ_{33}	σ_{12}	σ_{13}	σ_{23}
NFG600	Polishing	-221.3	-215.0	-12.3	-17.8	-8.2	-0.1
	Grinding	352.6	167.7	-2.0	5.4	-26.1	1.0
SM490	Polishing	-182.8	-164.6	36.3	-18.7	-8.0	0.9
	Grinding	378.3	175.5	21.1	9.4	-30.5	2.4

Table 6. Results by cos-ψ method of processed surface [MPa, MPa/μm].

		σ_{110}	σ_{220}	A_{11}	A_{22}	A_{33}
NFG600	Polishing	-350.4	-276.9	95	37.6	8.5
	Grinding	387.6	125.8	-31.9	39.5	0.8
SM490	Polishing	-280.3	-145.6	74.8	-25.7	17.4
	Grinding	403.6	94.5	-26.6	71.2	14.3

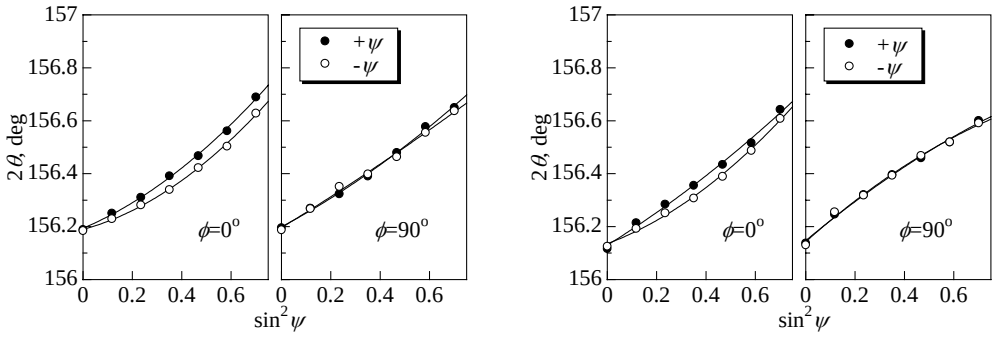

(a) NFG600-polishing. (b) SM490-polishing.

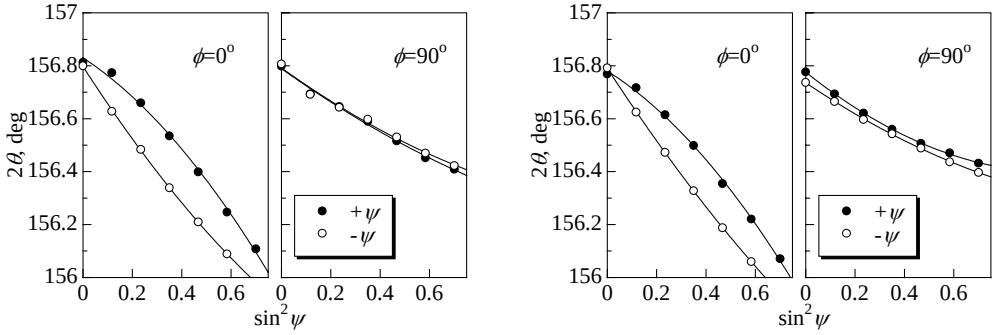

(c) NFG600-grinding. (d) SM490-grinding.

Figure 3. 2θ-$\sin^2\psi$ diagrams obtained by stress measurement.

Figure 4. Distribution of normal stress σ_{33} to depth.

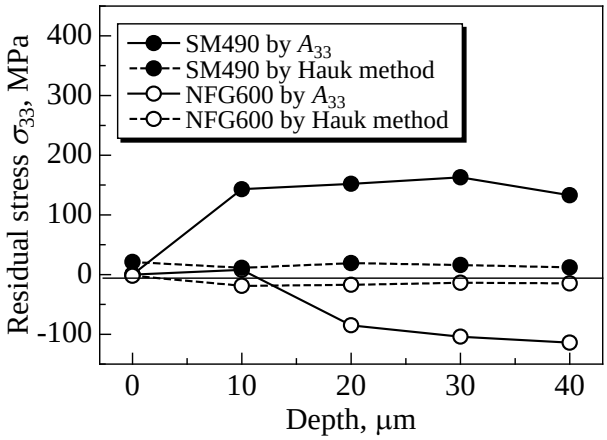

Summary

The fine-grained rolling steels NFG600 and the conventional usual rolling steels SM490 were processed by sand paper polishing and mechanical grinding to compare the residual stress generated after processing. About residual stresses of σ_{11} and σ_{22}, tensile stresses were generated with grinding. However, as for σ_{33}, the stress of NFG600 was almost compressive up to 40 μm, though that of SM490 was tensile. In addition, the change of stress from tension to compression was confirmed in the NFG600 specimen with the multi axial stress analysis using cos-ψ method.

References

[1] Information on http://www.nakayama-steel.co.jp/menu/product/nfg.html

[2] T. Hanabusa, K. Nishioka and H. Fujiwara: Z. Metallkde, Bd. 74, H. 5 (1983), pp. 307-313

[3] I.C. Noyan and J.B Cohen: *Residual Stress* (Springer-Verlag New York Inc., Germany 1987).

[4] Y. Yoshioka, T. Sasaki and M. Kuramoto: Advances in X-ray Analysis, Vol. 28 (1985), pp. 255-264